Chemical Science

ROYAL SOCIETY OF CHEMISTRY

EDGE ARTICLE

View Article Online
View Journal | View Issue

Cite this: *Chem. Sci.*, 2026, **17**, 6653

All publication charges for this article have been paid for by the Royal Society of Chemistry

High brightness in bis(tri-isopropylsilyl)ethynyl-functionalized polycyclic aromatic hydrocarbons: localized representation *versus* Clar's model

Kais Dhbaibi,[a] Huong Le Thi,[ab] Jérôme Marrot,[a] Masahiro Hayakawa,[c] Masashi Mamada[c] and Michel Frigoli*[a]

Recent studies on acenes have highlighted a localized representation (LR) of aromatic sextets, challenging Clar's classical model of migrating sextets. Here, we extend this framework to *peri*-fused systems by investigating bis(tri-isopropylsilyl)ethynyl (TIPS)-functionalized polycyclic aromatic hydrocarbons (TIPS-PAHs) namely TIPS-anthanthrene (**TIPS-ATT**), TIPS-pyranthrene (**TIPS-PYR**) and TIPS-dibenzo[pyranthrene] (**TIPS-DBPYR**) as test beds for LR. Crystal structures provide direct evidence for determining the Fries canonical structures, with bond lengths and bond length alternation (BLA) at the zig-zag edge offering robust criteria for positioning aromatic sextets. While NICS and HOMA indices are broadly consistent with these assignments, their interpretation should be considered with some caution. Optical studies reveal progressive bathochromic shifts (491–599 nm) with increasing conjugation, but absorption strength and fluorescence quantum yield depend critically on the mode of π-extension: catacondensation enhances brightness, whereas linear extension diminishes it. Remarkably, **TIPS-PYR** combines a record molar absorption coefficient (>200 000 M^{-1} cm^{-1}) with a high fluorescence quantum yield ($\Phi_F = 0.93$), yielding a molar brightness comparable to giant nanoribbons. Stability assays show that **TIPS-ATT** and **TIPS-PYR** are bench stable, whereas **TIPS-DBPYR**, despite reduced fluorescence efficiency, exhibits enhanced photostability relative to TIPS-pentacene (**TIPS-PEN**) and satisfies the energetic criterion for singlet fission. These findings establish LR as a robust framework for describing *peri*-fused PAHs, identify **TIPS-PYR** as an exceptionally bright dye, and position **TIPS-DBPYR** as a promising singlet fission material.

Received 2nd December 2025
Accepted 30th January 2026

DOI: 10.1039/d5sc09423b

rsc.li/chemical-science

Introduction

Over the past three decades, polycyclic aromatic hydrocarbons (PAHs) have been the focus of intensive investigation, spanning both fundamental questions of aromaticity and their emerging optoelectronic applications.[1–13] This modern interest is based on century old foundations, from Scholl's pioneering synthetic strategies to Clar's influential structural and aromaticity models.[14–16] Clar's sextet model, in particular, has long provided a powerful tool for rationalizing the interplay between aromatic stabilization, molecular stability and optical properties.[16] For planar PAHs with a unique Clar structure such as phenanthrene, pyrene and triphenylene, the representation is straightforward (Fig. 1a).[16,17] For systems describable by

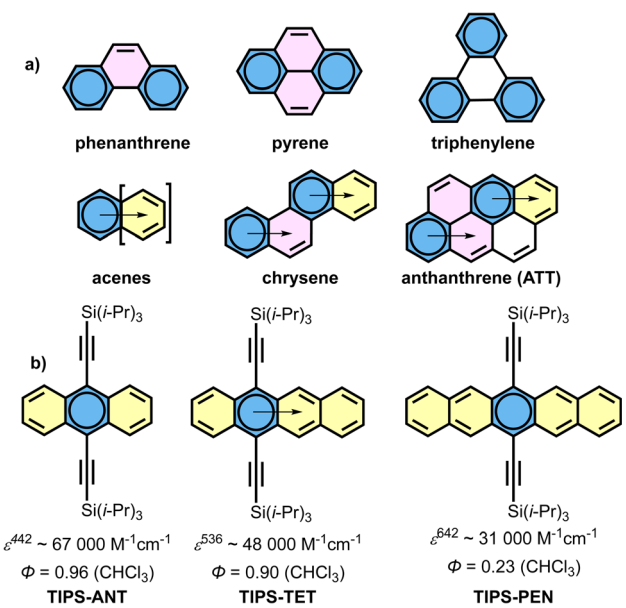

Fig. 1 (a) Clar representation of the selected PAHs; (b) localised representation (LR)[19] and optical properties of TIPS-acenes in chloroform solution.[20]

[a]*UMR CNRS 8180, UVSQ, Institut Lavoisier de Versailles, Université Paris-Saclay, 45 Avenue des Etats-Unis, 78035 Versailles Cedex, France. E-mail: michel.frigoli@uvsq.fr*
[b]*Department of Advanced Materials Science and Nanotechnology, University of Science and Technology of Hanoi (USTH), Vietnam Academy of Science and Technology (VAST), 18 – Hoang Quoc Viet, Ha Noi 11307, Vietnam*
[c]*Department of Chemistry, Graduate School of Science, Kyoto University, Kitashirakawa Oiwake-cho, Sakyo-ku, Kyoto 606–8502, Japan*

multiple Clar structures, Clar introduced the concept of migrating sextets, exemplified in acenes, chrysene, anthanthrene (**ATT**) (Fig. 1a) and related PAHs.[16,18] Yet the case of acenes has recently challenged the classical Clar picture. We recently proposed the localized representation (LR) of acenes, in which the aromatic sextet is centred in the middle of the molecules (Fig. 1b).[19] Accordingly, acenes can be viewed as symmetric linear extensions of benzene. The validity of this LR is supported by bond length alternation (BLA) analyses, which show that the zig-zag edges of acenes closely resemble those of *ortho*-quinoid acenothiophenes.[19,21] The LR highlights that acenes are aromatic compounds with a $4n + 2$ π-electron count along their periphery. Thus, despite their polycyclic structure, they can also be regarded as $4n + 2$ annulenes, not only by virtue of the alternating single and double bonds along the zig-zag edge, but also because this connectivity gives rise to a predominantly global perimetric ring current, as evidenced by the anisotropy of the induced current density (ACID) plots.[19] Complementary current density analyses based on the pseudo-π approach further indicate that, in addition to this dominant global current, acenes exhibit weaker (semi)local contributions.[22,23] It should be emphasized that unlike the classical representation of acenes based on a single Kekulé structure,[24,25] which no longer provides an adequate account of their ring current behaviour, the LR systematically incorporates all these components of the $4n + 2$ diatropic ring current (see the SI).[26] Moreover, resonance energy data derived from experimental heats of formation, which increase nearly linearly with ring number, underscore that stabilization is not fully delocalized across the backbone but instead reflects localized contributions.[27] In this way, the LR reconciles bond length alternation with energetic resonance stabilization and with both global and subsidiary current density contributions, characteristic of acenes.[28]

Acenes represent a particularly remarkable family of PAHs as each additional fused ring containing a *cis*-diene induces an exceptionally large bathochromic shift of nearly 100 nm in the absorption maximum. For instance, when functionalized with TIPS-ethynyl groups at the central ring, the absorption maxima are 442 nm for TIPS-anthracene (**TIPS-ANT**), 536 nm for TIPS-tetracene (**TIPS-TET**) and 642 nm for TIPS-pentacene (**TIPS-PEN**) in diluted chloroform solution (Fig. 1b).[20] However, both the molar absorption coefficient (ε) and the fluorescence quantum yield (Φ_F) decrease with increasing ring number, correlating with a progressive loss of aromatic stabilization from the dilution of the central aromatic sextet by the successive addition of *cis*-diene fragments (Fig. 1b). This pattern is also observed in the [*m*,2]*peri*-acenoacene family developed by Wu and coworkers, where ε and Φ_F decrease as the molecular structure becomes more laterally extended.[29] In this series, although the substituents are not located in the same position and therefore they are not strictly comparable, ε decreases roughly from 65 000 M^{-1} cm^{-1} for mesityl-anthanthrene (**Mes-ATT**) to 35 000 M^{-1} cm^{-1} for *peri*-pentacenopentacene (**PPP**) and Φ_F decreases from 56 to 32%, respectively. Recently, we synthesized **TIPS-PPP**, which exhibits a 26-fold increase in stability compared to **TIPS-PEN**,[28] maintaining the same 2D π–π brickwork molecular packing and a 6-fold increase in charge transport in organic field-effect transistor (OFET) devices.[19,30] With absorption at 726 nm and a ε of 85 000 M^{-1} cm^{-1}, the optical properties of **TIPS-PPP** suggest that **TIPS-ATT**, a smaller analogue, may have a ε exceeding 100 000 M^{-1} cm^{-1}, a remarkable value for a small PAH (Fig. 2). The optical properties of **TIPS-ATT**, beyond its absorption spectrum, remain unknown despite its use as a donor in OPV devices and as an active layer in OFETs.[31,32] Even more striking, Morin and coworkers recently reported dibenzo [*a*,*l*]*peri*-tetracenotetracene derivatives (**DBPTT**) with an ε of 168 000 M^{-1} cm^{-1} at 611 nm when functionalized with TIPS groups, although fluorescence data were not reported.[33] This finding suggests that TIPS-pyranthrene (**TIPS-PYR**), a smaller analogue, could possess an even stronger ε, making it a very high brightness dye if combined with high fluorescence quantum yield (Fig. 2).[31]

In this context, **TIPS-ATT** and **TIPS-PYR**, the latter of which can be regarded as cata-extensions of the **ATT** core along the *a*,*j* faces, emerge as particularly valuable cases due to their multiple Clar structures, making them ideal test beds for the localized representation (LR). To further extend this framework, we also investigated TIPS-dibenzo[pyranthrene] (**TIPS-DBPYR**), a lateral expansion of the **PYR** core (Fig. 2), in order to elucidate the impact of cata *versus* linear extension in PAHs on their optoelectronic properties. This study reports their synthesis, optoelectronic properties, stability, and crystal structures. The latter were analysed in depth using structural parameters such as bond lengths and bond length alternation (BLA), along with "aromaticity indices" including nucleus-independent chemical shift (NICS)[34] and the harmonic oscillator model of aromaticity (HOMA).[35]

Results and discussions

Synthesis

TIPS-ATT can be synthesized in a single step from anthanthrone (Scheme 1).[30] Using the classical lithium salt of TIPS, the yield was limited to 15%, reflecting the well-known competition between 1,2- and 1,4-addition pathways on anthanthrone.[36] To favour the desired 1,2-addition, we carried out the reaction in the presence of $LaCl_3$ LiCl, as previously applied in the synthesis of **TIPS-PPP**, which significantly improved the yield.[19]

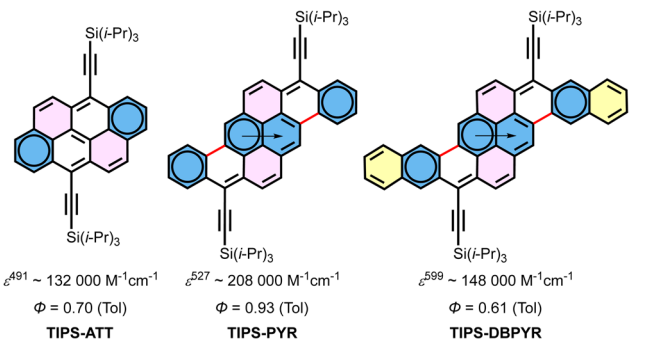

Fig. 2 Localized representations of the molecules investigated in this study and their associated optical properties.

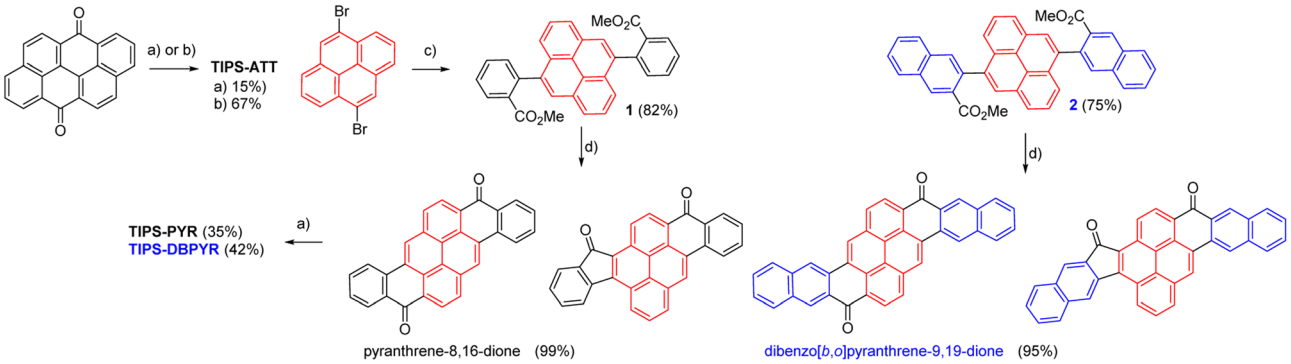

Scheme 1 Synthesis of **TIPS-ATT**. (a) (1) tri-isopropylsilylacetylide, THF, −10 °C to rt, (2) $SnCl_2$/HCl, rt; (b) tri-isopropylsilylacetylide, $LaCl_3 \cdot 2$ LiCl, THF, −10 to 0 °C and (2) $SnCl_2$/HCl, rt. Synthesis of **TIPS-PYR** and **TIPS-DBPYR**. (c) Ester boronic derivatives, $Pd_2(dba)_3$, S-Phos, K_3PO_4, toluene/water, 100 °C; (d) TfOH, 1,2-dichloroethane, 90 °C.

Pyranthrone is a commercially available product that can be synthesized by two main methods: the first starts with 2,2′-dimethyl-[1,1′-bianthracene]-9,9′,10,10′-tetraone as the starting material and the second starts with pyrene-1,6-diylbis(phenylmethanone), which then undergoes a Scholl reaction. In the Scholl reaction, when starting from pyrene-1,6-diylbis(naphthalen-2-ylmethanone), cyclization occurs specifically at position 1 of the naphthalene ring.[37] Consequently, none of these methods is suitable to obtain the extended version of pyranthrone. Given that the first two Friedel–Crafts acylations of pyrene occur at positions 1 and 6, compounds **1** and **2** emerged as convenient precursors for obtaining large diones (Scheme 1). These two compounds were obtained in good yield through a Suzuki reaction between 5,10-dibromopyrene and the corresponding boronic esters.[38] The double intramolecular Friedel–Crafts acylation/cyclization using triflic acid as an activator proceeded smoothly.[39–42] However, infrared spectra of both insoluble compounds revealed the presence of two carbonyl stretches: more intense bands at 1641 and 1648 cm^{-1}, characteristic of a six-membered ring (6-MR) aromatic ketone, and less intense bands at 1704 and 1691 cm^{-1}, respectively, indicative of a five-membered ring (5-MR) aromatic ketone (see the SI). Despite this, the two targeted diones having two 6-MRs are likely the major products, as the C=O stretch of 5-MR is typically much more intense compared to that of 6-MR (see the SI).[38] The regioselectivity reflects a competition between electronic and steric factors. The intrinsic reactivity of the 1,6-positions in pyrene rationalizes their role as the preferred electrophilic sites, even though they are also the most sterically hindered. Following the first cyclization at C1, the electrophilic susceptibility of C6 is attenuated, thereby shifting partial activation toward C4, which represents the most sterically accessible alternative site. Addition of TIPS-acetylide to either the pyranthrone or dibenzopyranthrone mixture afforded **TIPS-PYR** and **TIPS-DBPYR**, respectively, in moderate yields. The structures of all three compounds were unambiguously confirmed by NMR spectroscopy, high-resolution mass spectrometry (HRMS) and single crystal X-ray crystallography (see the SI).

X-ray crystallographic analysis and localised representation

The crystal structures of **TIPS-ATT** and **TIPS-PYR** have already been determined.[29,30] However, the reliability factor (*R*-factor) exceeds 0.1, precluding meaningful discussion of bond lengths. Attempts to obtain higher quality crystals of **TIPS-ATT** were unsuccessful, whereas crystals of sufficient quality were obtained for **TIPS-PYR** ($R = 0.060$) and **TIPS-DBPYR** ($R = 0.057$), enabling reliable structural analysis. For structural comparison, we therefore refer to the crystal structures of **Mesityl-ATT** and the parent **ATT**.[27,43]

Since the LR of acenes has been rationalized by analogy with the bond lengths observed in both acenes and acenothiophenes,[19] we begin with pyrene, phenanthrene and chrysene as reference systems, together with naphthalene (Fig. 3). In the crystal structures, the bonds depicted in blue are shorter than their neighbours. By analogy with acenes, these shortened bonds can be assigned as formal double bonds, thereby giving rise to a specific Kekulé resonance structure (Fig. 3 and 4). This latter corresponds to the Fries structure, in which the maximum number of rings share a double bond at the fusion and can therefore be formally represented as having six internal π-electrons.[44,45] Consequently, the preferred representation of PAHs using single and double bonds should be the Fries structure, since it corresponds most closely to the crystallographic data. While Graovac *et al.* introduced the Kekulé index and suggested that the Fries structure has the dominant contribution in the ground state,[46] the Fries structure of naphthalene likely accounts for 50% of the ground state. This is because the rings of naphthalene can be regarded as a resonance hybrid between a delocalized aromatic sextet and a *cis*-diene, in agreement with the Clar model (Fig. 3). This interpretation is supported by bond length alternation analysis: the peripheral BLA of naphthalene corresponds to the average of an aromatic sextet (0) and a *cis*-diene (0.074, as in anthracene), yielding a value of 0.037, which is in close agreement with the observed BLA of 0.043.[19] It should be noted that Fries assumed, in the case of anthracene, that the oscillation of double bonds was confined to the central ring while the outer rings retained fixed double bonds.[43] This arrangement corresponds directly to the LR of anthracene (Fig. 1).

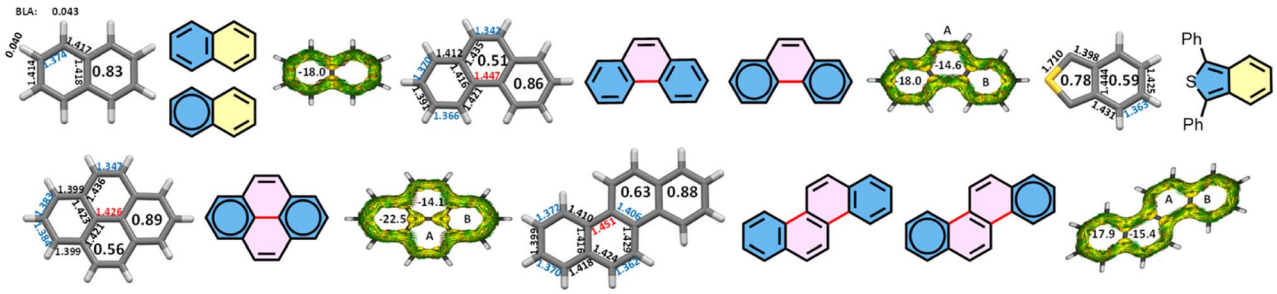

Fig. 3 Crystal structures of naphthalene,[47] pyrene,[48] phenanthrene,[49] chrysene[50] and 1,3-diphenylbenzo[*c*]thiophene[21] (phenyl rings removed) with bond lengths and HOMA values inside the rings. The deduced Fries structures and the corresponding Clar structures and LR for chrysene. ACID plots and NICS(1.7)πzz inside the rings of molecules with optimized structures.

Pyrene and phenanthrene each possess a single Clar structure, whereas chrysene has three. For pyrene and phenanthrene, there is broad consensus that the Clar structure with two aromatic sextets located in the terminal rings provides the most accurate description.[18] Pyrene belongs to the D_{2h} point group, and as a consequence, the bond lengths in the outer rings B are inherently delocalized. This delocalization makes the Clar structure particularly evident: the outer rings B are represented as aromatic sextets, while ring A contains a localized double bond of 1.347 Å. The bond length distribution thus provides direct structural support for the Clar structure of pyrene. Accordingly, HOMA and NICS values are highest for rings B. Notably, the single bond highlighted in red is as short as 1.426 Å. Pyrene, with 16 π-electrons (4n), exhibits a strong global diatropic ring current (clockwise) of 14 π-electrons (4n + 2), together with two weaker local ring currents of 6 π-electrons, each around rings B, as revealed by the acid plot.

For phenanthrene, the Fries structure can be deduced from the alternating lengths of the external bonds in rings B. These bond lengths are very similar to those of naphthalene, with the notable exception of the C2–C3 bond, which measures 1.391 Å in phenanthrene *versus* 1.414 Å in naphthalene (Fig. 3), resulting in a slightly higher HOMA value. Owing to this shorter bond, three adjacent bonds within rings B fall within a narrow range (1.366–1.391 Å; BLA = 0.025 Å), lower than that observed in naphthalene (BLA = 0.040 Å). Since naphthalene is represented as a resonance hybrid between a delocalized aromatic sextet and a *cis*-diene (Fig. 3), rings B of phenanthrene are most appropriately described as delocalized aromatic sextets. The outer bond lengths of rings A, which closely resemble those observed in pyrene, further support the placement of the aromatic sextet in rings B. As in pyrene, the NICS and HOMA values for rings B corresponding to the aromatic sextet are higher than those for rings A. The red bond connecting the two phenyl rings measures 1.447 Å and a comparison with the corresponding bond in pyrene (1.426 Å) illustrates how single bond lengths are strongly modulated by their molecular environment, just as the lengths of single and double bonds are modulated in acenes.[19] Phenanthrene, with 14 π-electrons, sustains a global diatropic ring current of 14 π-electrons in the ACID plot.

Chrysene can be analyzed in the same way. The bond lengths in rings B closely resemble those in phenanthrene, thereby supporting the placement of the aromatic sextets in the terminal rings, as confirmed by comparable HOMA and NICS values. This interpretation is further reinforced by the single bond connecting rings B and A (highlighted in red, 1.451 Å), which is nearly identical to the corresponding bond in phenanthrene (1.447 Å) and consistent with their cata-condensed arrangement. Moreover, while the BLA of the outer bonds in

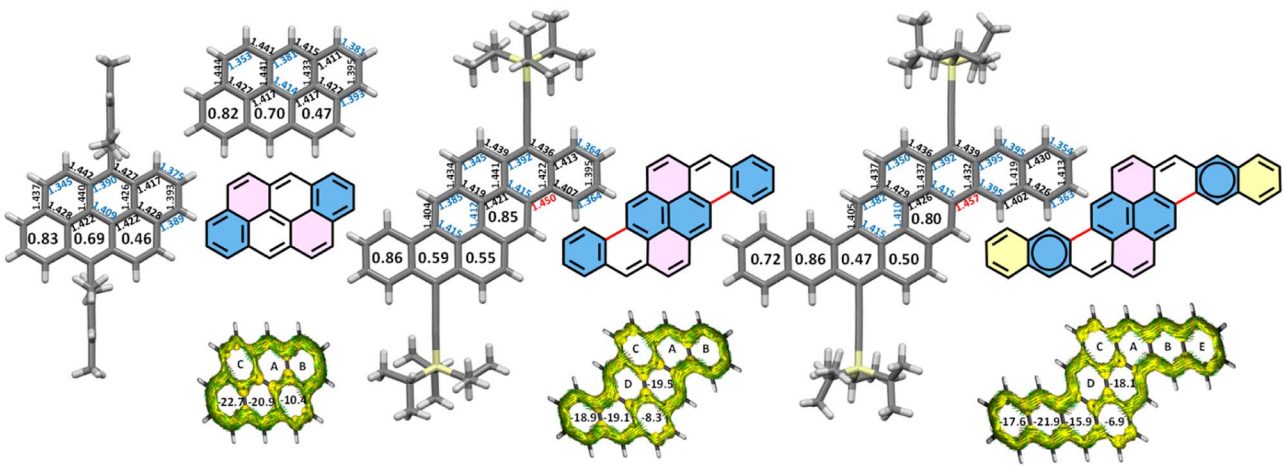

Fig. 4 Crystal structures of **Mes-ATT**,[27] **ATT**,[43] **TIPS-PYR** and **TIPS-DBPYR** with bond lengths and HOMA values inside rings, deduced Fries structures and ACID plots and NICS(1.7)πzz inside the rings of parent PAHs with optimized structures.

rings B is slightly lower than in phenanthrene, leading to a higher HOMA value, similar outer bond lengths are also observed in the 6-MR of benzo[*c*]thiophene (Fig. 3).[21] Accordingly, chrysene can be represented as one LR. While phenanthrene and pyrene can be considered as biphenyls linked by one or two ethenyl spacers, respectively, chrysene can be considered a *trans*-stilbene with two ethenyl bridges. Chrysene, with 18 π-electrons, shows a global ring current of 18 π-electrons in the ACID plot.

The Clar representation of **ATT** already indicated that rings C contain localized bonds since Clar originally regarded **ATT** as an extension of pyrene (Fig. 1a).[16] This assignment is consistent with the highest BLA at the periphery and the lowest HOMA and NICS values observed for rings C (Fig. 4). However, as discussed above, smaller cata-condensed PAHs are more appropriately described as arenes bridged by two ethenyl spacers, in line with the general tendency of nature to favour symmetry. From this perspective, **ATT** should therefore be regarded not as an extension of pyrene but rather as an extension of chrysene. Accordingly, the LR of **ATT** can be directly deduced from that of chrysene and both HOMA and NICS values fully support this assignment. More specifically, the BLA of the outer bonds in rings B is similar to or lower than that observed in chrysene with both molecules sharing the same symmetry. In contrast, the reduced HOMA values originate from relatively long intra-annular bonds, in comparison to pyrene, which exhibits the same structural motif. Nevertheless, the NICS value of ring B remains comparable to that of pyrene, consistent with its designation as an aromatic sextet within an identical environment of two neighbouring rings. The BLA at the periphery of rings A is significantly lower than in chrysene, reflecting their central position and the resulting higher degree of conjugation, as observed in acenes.[19] Nevertheless, the BLA of rings A (0.034–0.037 Å) remains higher than that of the second ring of pentacene (0.026 Å), indicating that the bonds in rings A are localized. Owing to this relatively low BLA and the fact that each ring A is fused to three different neighbours, their NICS values are higher than those of pyrene, in which the corresponding rings are fused to only two different neighbours. Although **ATT** is an aromatic compound with 22 π electrons, the ACID plot reveals two distinct 18 π-electron ring current circuits when only the symmetry allowed pathways are considered: one following the periphery and the other bifurcated, corresponding to the chrysene subunit of the π-structure. This dual circuit confirms that **ATT** is best described as an extended version of chrysene. The chrysene contribution is further evident in the shape of the HOMO orbital (see the SI).

Considering all of the above, the Fries structure of **TIPS-PYR** together with its molecular symmetry and the structural parameters at the zig-zag edge (bond lengths and BLA values) and HOMA index, places the aromatic sextets on rings B and D (Fig. 2). Although the HOMA and NICS values of rings B are comparable to or higher than those of phenanthrene, which correspond to a phenanthrene-type aromatic sextet, the NICS values of rings A are very similar to those of rings B and could be misinterpreted as a migration of the sextet between rings A and B. This apparent "magnetic delocalisation" results from the local environment of ring A: its three non-equivalent neighbours reinforce its local magnetic susceptibility. The combined evidence from the structure (bond lengths, BLA and HOMA) therefore continues to support the LR with sextets localized on rings B and D (Fig. 2). Moreover, **PYR** can be regarded as an extended fulminene ([6]-phenacene): a fulminene core bridged by two ethenyl spacers. **PYR** is an aromatic system with 30 π-electrons (4n + 2), but the ACID plot reveals two distinct 26 π-electron ring current circuits: one delocalized along the periphery and another bifurcated pathway around the fulminene subunit. Moreover, fulminene itself can be seen as a 2,6-diphenylnaphthalene bridged by two ethenyl spacers.[18]

In the case of **TIPS-DBPYR**, all structural parameters (bond lengths and BLA) and "aromaticity indices" (HOMA and NICS) consistently place the aromatic sextets on rings B and D. Thus, the LR of **TIPS-DBPYR** can be seen in Fig. 2.

Ultimately, crystal structures provide a direct means of identifying the Fries structures. Bond lengths and bond length alternation (BLA) analysis at the zig-zag edge offer a robust criterion for positioning aromatic sextets. In the present series, NICS and HOMA values are largely consistent with these structural attributions, except in the case of **PYR**, where NICS overestimates the local aromaticity of a ring due to the high number of neighboring rings. HOMA may likewise underestimate local aromaticity when internal bonds are elongated by conjugation, as observed for the central ring in pentacene.[51] These discrepancies highlight the need to interpret local aromaticity indices with caution, and the placement of aromatic sextets cannot be deduced from a single criterion such as NICS or HOMA in molecules that possess more than one Clar structure.

It should be noted that in phenanthrene, chrysene and anthanthrene, electrophilic substitution occurs preferentially at the central rings bearing double bonds, whereas in pyrene and in the acenes, the most reactive sites correspond to the rings hosting aromatic sextets.[52,53] This demonstrates that the reactivity of PAHs cannot be rationalized solely in terms of their ground state electronic structures. While the computed thermodynamic stability of PAH adduct intermediates and the average local ionization energy (ALIE) provide a reasonable prediction of reactivity,[51] the calculated spin density distribution of the triplet state (the singlet state being inaccessible for closed-shell systems) may serve as an even more reliable predictor of reactivity, as it likely resembles the electronic structure of the transition state.[54] For **ATT**, **PYR** and **DBPYR**, the most reactive site is ring A, which bears the highest spin density at the zig-zag edge, as illustrated in Fig. 5. The Clar structure of the diradical is in good agreement with these calculations.

Electrooptical properties, stability and theoretical calculations

The optical properties and stability were investigated in toluene solution (Fig. 6 and Table 1). The smaller analogue, **TIPS-ATT**, exhibits an absorption maximum at 491 nm, while **TIPS-PYR** is red shifted by 36 nm to 527 nm. A further linear extension from **TIPS-PYR** to **TIPS-DBPYR** produces an even more pronounced

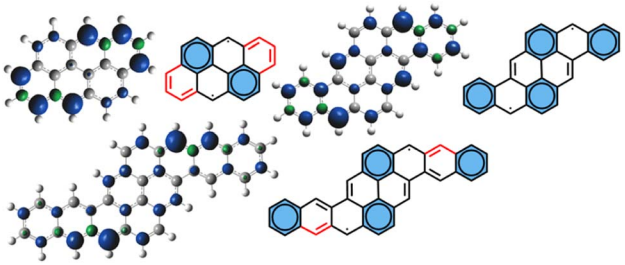

Fig. 5 Triplet spin density and Clar structures showing the main delocalization along red highlighted bonds.

red shift of 72 nm, yielding an absorption maximum at 599 nm. Thus, each additional ring induces a red shift of approximately 36 nm, in sharp contrast to the ~100 nm increments typically observed in acenes. These progressive bathochromic shifts arise from the concomitant destabilization of the HOMO and stabilization of the LUMO, amounting to 0.09 eV from **TIPS-ATT** to **TIPS-PYR** and 0.15 eV from **TIPS-PYR** to **TIPS-DBPYR**, thereby narrowing the frontier orbital gap (Table 1). The calculated HOMO–LUMO gaps for the three molecules are in very good

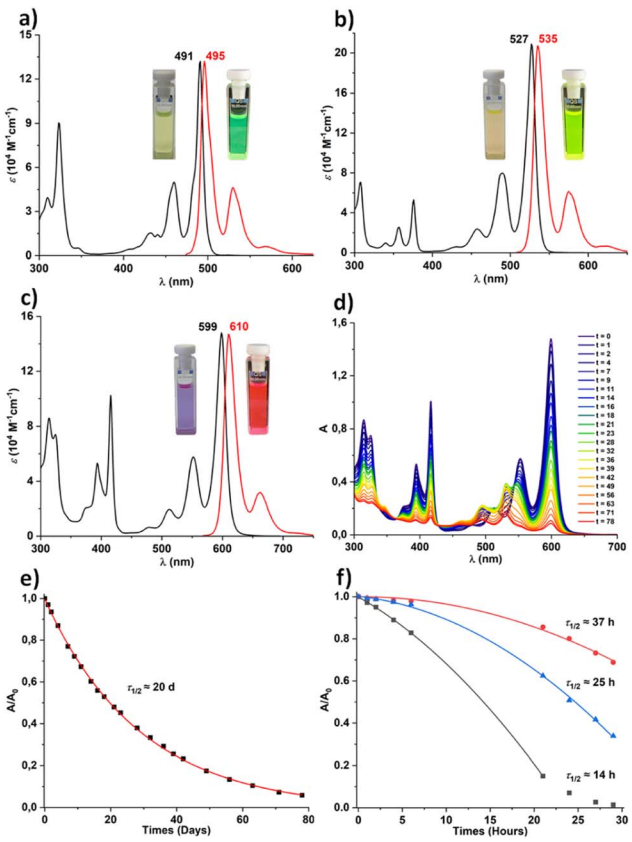

Fig. 6 Absorption and fluorescence spectra of (a) TIPS-ATT, (b) TIPS-PYR and (c) TIPS-DBPYR accompanied by photographs of the corresponding cuvettes under ambient light (left) and under 365 nm UV illumination (right); (d) UV/vis spectral evolution and (e) change of absorbance at 599 nm over time under ambient laboratory conditions for TIPS-DBPYR ($[C] = 1 \times 10^{-5}$ M in toluene); (f) change of absorbance at their own λ_{max} over time in toluene with 365 nm light for TIPS-ATT (red), TIPS-PYR (blue) and TIPS-DBPYR (black).

Table 1 Optoelectrochemical properties of the molecules

Compounds	TIPS-ATT	TIPS-PYR	TIPS-DBPYR
λ_{max} [nm][a]	491	527	599
ε_{max} [M^{-1} cm^{-1}][b]	132 000	208 000	148 000
ε_{365} [M^{-1} cm^{-1}][b]	1000	7100	11 700
λ_{em} [nm][c]	495	535	610
Φ_F (air)/Φ_F (N_2) [%][d]	0.64/0.70	0.86/0.93	0.51/0.61
$\Phi_F \times \varepsilon_{max}$ (N_2)[e]	92 400	193 400	90 300
τ_F (air)/τ_F (N^2) [ns][f]	2.37/2.65	2.20/2.52	5.34/6.24
k_r (N_2) [s^{-1}][g]	2.64×10^8	3.69×10^8	9.77×10^7
k_{nr} (N_2) [s^{-1}][h]	1.13×10^8	2.06×10^7	6.25×10^7
E_g^{opt}[i]	2.48 (499)	2.30 (538)	2.02 (614)
$E(S_1)$ [eV] (nm)[j]	2.51 (493)	2.33 (531)	2.05 (604)
$E(S_1)$ [eV] (nm)[k]	2.58 (480)	2.40 (517)	2.10 (591)
f[k,l]	0.98	1.80	1.62
$E(T_1)$ [eV] (nm)[k]	1.35 (918)	1.29 (961)	1.03 (1204)
$\Delta E([S_1]-[T_1])$ [eV][k]	1.23	1.11	1.07
HOMO/LUMO [eV][l]	−5.15/−2.67	−5.06/−2.76	−4.91/−2.91
H–L gap [eV] (nm)[m]	2.48 (500)	2.30 (540)	2.00 (620)
y_0[n]	0.30	0.34	0.42

[a] Absorption maximum. [b] Molar absorption coefficient. [c] Emission maximum. [d] Quantum yield of fluorescence determined in air and under N_2. [e] Molar fluorescence brightness calculated under N_2. [f] Fluorescence lifetime. [g] Radiative rate constant calculated as $k_r = \Phi_F/\tau_F$. [h] Non-radiative rate constant calculated as $k_{nr} = (1 - \Phi_F)/\tau_F$. [i] Optical band gap estimated from absorption onset (tangent). [j] Deduced from the intersection between absorption and emission spectra. [k] TD-DFT calculation at the M062X/6-311+G(d,p) level using optimized geometry calculated at the B3LYP/6311 + G(d,p) level. [l] Oscillator strength. [m] Calculated at the B3LYP/6311 + G(d,p) level. [n] Biradical character calculated at the BS-UHF/6-31G(d,p) level.

agreement with the optical band gap (E_g^{opt}) obtained from the absorption onset using the tangent method (Table 1). As expected, **TIPS-ATT** exhibits a higher ε than the laterally extended **TIPS-PPP** (85 000 M^{-1} cm^{-1}), reaching a remarkable value of 132 000 M^{-1} cm^{-1}. Even more striking, **TIPS-PYR** displays an ε exceeding 200 000 M^{-1} cm^{-1} underscoring the exceptional light harvesting capability of this system. In contrast, lateral extension of the **PYR** core to **TIPS-DBPYR** reduces ε to 148 000 M^{-1} cm^{-1}, highlighting the sensitivity of absorption strength to the mode of π-extension (cata *vs.* linear). Within this series, the fraction of rings that can be described as Clar sextets increases upon cata extension (2/6 in **ATT** *vs.* 3/8 in **PYR**) correlating with the observed enhancement in ε, whereas this fraction decreases with the introduction of *cis*-diene units upon linear extension (3/8 **PYR** *vs.* 3/10 **DBPYR**), which in turn correlates with a reduction in ε. TD-DFT calculations of these allowed $S_0 \rightarrow S_1$ transitions reproduce this trend, with **TIPS-PYR** exhibiting the highest oscillator strength ($f = 1.80$), while **TIPS-ATT** shows the lowest ($f = 0.98$). In relative terms, however, the calculated intermediate f value of 1.62 for **TIPS-DBPYR** appears to be significantly overestimated compared to the experimental value. Among the three compounds, **TIPS-PYR** shows the highest absolute quantum yield of fluorescence ($\Phi_F = 0.93$) in deoxygenated solution, while **TIPS-DBPYR** has the lowest ($\Phi_F = 0.61$). By contrast, **TIPS-ATT** has an intermediate value ($\Phi_F = 0.70$). Notably, the formal molar fluorescence brightness of

TIPS-PYR ($\varepsilon\Phi_F = 193\,000\ M^{-1}\ cm^{-1}$) is comparable to that reported for giant nanoribbons (GNRs).[55] **TIPS-PYR** thus stands out as one of the brightest dyes among polybenzenoid compounds. By contrast, **TIPS-ATT** and **TIPS-PYR** display $\varepsilon\Phi_F$ values of approximately 90 000 M^{-1} cm^{-1}, which are comparable to those of well-established fluorescent benchmarks such as pyrromethene dyes and perylenediimides.[56,57] It should be noted that *peri*-acenoacenes generally display lower Φ_F values compared to their acene counterparts. **TIPS-ANT** exhibits a Φ_F of 0.96, whereas **TIPS-ATT** shows a reduced value of 0.70 and similarly **TIPS-PEN** ($\Phi_F = 0.44$) is reduced relative to **TIPS-PPP** ($\Phi_F = 0.27$) in diluted toluene solution.[19] The reduction of Φ_F for **TIPS-ATT** can be attributed to the competition between fluorescence and intersystem crossing (ISC) from the first excited singlet state (S_1), a process that has previously been demonstrated in **ATT** derivatives.[58,59] For all compounds, the fluorescence quantum yield (Φ_F) increased under deoxygenated conditions, indicating the quenching of S_1 by molecular oxygen ($^3O_2$).[60] This effect was most pronounced for **TIPS-DBPYR**, which can be ascribed to its comparatively smaller radiative decay rate constant and larger molecular size (Table 1).[60] As recently demonstrated for perylenediimides, all compounds studied here are intrinsically capable of producing singlet oxygen ($^1O_2$) from both S_1 and the first triplet excited state (T_1).[60] From S_1, this process is energetically allowed since the gap $\Delta E = E(S_1)$–$E(T_1)$ exceeds 0.976 eV, while from T_1, it is enabled because $E(T_1)$ lies above the excitation energy of $^3O_2 \rightarrow {}^1O_2$ (0.976 eV) (Table 1). In other words, under illumination, these molecules act as photosensitizers, generating reactive $^1O_2$ with **TIPS-DBPYR** likely being the most efficient. Moreover, according to the calculation, energetically, only **TIPS-DBPYR** satisfies the singlet fission criterion with $E(S_1) \geq 2E(T_1)$ providing a near isoenergetic driving force for the formation of the correlated triplet pair. Given that **TIPS-DBPYR** also exhibits markedly greater photostability than **TIPS-PEN** (*vide infra*), it emerges as a particularly promising candidate for singlet fission applications.[61]

Stability tests were performed in toluene solution ($[C] = 1 \times 10^{-5}$ M) under ambient laboratory conditions with permanent light exposure. The stability studies reveal that while **TIPS-ATT** and **TIPS-PYR** remain intact under these conditions, **TIPS-DBPYR** undergoes slow degradation with a half-life ($\tau_{1/2}$) of 20 days (Fig. 6d and e and SI). The monoexponential decay at 599 nm confirms a first-order kinetic process, excluding the involvement of secondary degradation pathways that could accelerate $^1O_2$ generation. It should be noted that **TIPS-DBPYR** is 20 times more stable than **TIPS-PEN** ($\tau_{1/2} = 1.4$ days) studied under the same conditions.[19] As illustrated in Fig. 6d, the original absorption bands of **TIPS-DBPYR** progressively decrease, while new bands emerge at 531, 495, and 462 nm. The intensities of these new bands grow steadily up to 28 days before subsequently declining. The progressive decrease of the three bands in their relative intensities with energy is characteristic of acene-like chromophores. The new spectral features are tentatively attributed to endoperoxide formation localized on one of the aromatic sextets (rings B) (see the SI). TD-DFT calculations on this degradation product further support this assignment (see the SI). By contrast, exposure to two 6 W bench lamps at 365 nm resulted in degradation of all compounds (Fig. 6f and SI). The decay monitored at each compound's λ_{max} could well be fitted with a quadratic function, indicating an acceleration of the degradation process under these conditions (Fig. 5e). This can result from the formation of ketone-based photoproducts, as previously shown in **TIPS-PPP**.[19] Among the series, **TIPS-ATT** proved to be the most robust ($\tau_{1/2} = 37$ h), **TIPS-DBPYR** was the least stable ($\tau_{1/2} = 14$ h) and **TIPS-PYR** exhibited intermediate stability ($\tau_{1/2} = 25$ h). By analogy with acenes, where stability diminishes as the number of fused rings increases relative to the single Clar sextet, the predicted stability order is **TIPS-PYR** (3/8) > **TIPS-ATT** (2/6) > **TIPS-DBPYR** (3/10) (Fig. 2). Experimentally, however, an inversion is observed between **TIPS-ATT** and **TIPS-PYR**. Under our test conditions, this discrepancy indicates that factors beyond the Clar sextet count must be considered. Although a clear correlation exists between biradical character (y_0)[62,63] and thus the HOMO–LUMO gap (Table 1) and stability, the dominant factor in this series is likely photochemical: **TIPS-PYR** and **TIPS-DBPYR** exhibit ε at 365 nm that are approximately seven and eleven times higher, respectively, than that of **TIPS-ATT**, thereby accounting for their reduced stability (Table 1). However, there is no strict correlation between ε and stability, only a general trend. Additional insight is provided by the nature of the oxidation photoproducts. Upon photooxidation, **TIPS-PYR** derivatives gain an extra Clar sextet (increasing from three to four), leading to stabilization that is more significant than in the case of **TIPS-ATT**, whose Clar sextet count remains unchanged (two to two) (Fig. 5). Accordingly, the observed stability trend can be rationalized by the combined influence of photophysical properties (ε and τ_F) and the relative thermodynamic stability of the resulting photoproducts.[64]

Conclusions

This work demonstrates that chrysene, anthanthrene and pyranthrene can be consistently represented as localized structures with the aromatic sextets positioned on the outer rings. By analogy with phenanthrene and pyrene, which can be regarded as biphenyls with one or two ethenyl spacers, respectively, chrysene, anthanthrene and pyranthrene may be viewed as derivatives of *trans*-stilbene, chrysene and fulminene cores, each extended by two ethenyl spacers. Crystal structures provide direct evidence of determining the Fries structures. Representing polybenzenoid compounds with single and double bonds should therefore follow the Fries model. Bond lengths and bond length alternation (BLA) at the zig-zag edge offer robust criteria for positioning aromatic sextets. While NICS and HOMA indices are broadly consistent with these assignments, their interpretation requires caution. Photophysical studies reveal clear design rules: cata-condensation enhances brightness, as exemplified by **TIPS-PYR** with record molar brightness, whereas linear extension reduces emission efficiency but potentially enables singlet fission functionality, as in **TIPS-DBPYR**. Stability trends are further rationalized by the interplay between the molar absorption coefficient, radiative lifetime and the relative thermodynamic stabilization of oxidation photoproducts.

Beyond highlighting the localized structure of *peri*-fused systems, this study identifies **TIPS-PYR** as an exceptionally bright dye and **TIPS-DBPYR** as a potentially robust singlet fission material, thereby expanding the molecular design space for next-generation optoelectronic devices.

Author contributions

K. D. and K. L. T. conducted the synthesis and the study of the optical properties and managed the data. J. M. and M. H. obtained the crystal structures and managed the data. M. M. performed theoretical calculations, managed the data and carried out the review. M. F. contributed to conceptualization, writing, review and editing and project administration. All authors have read and approved the final version of the manuscript.

Conflicts of interest

There are no conflicts to declare.

Data availability

CCDC 2503087, 2503088 and 2504051 contain the supplementary crystallographic data for this paper.[65a–c]

The data supporting this article have been included as part of the supplementary information (SI). Supplementary information: experimental procedures, characterization data for the synthesized compounds and theoretical calculations. See DOI: https://doi.org/10.1039/d5sc09423b.

Acknowledgements

The synchrotron X-ray crystallography experiments were performed at the BL40XU beamline of SPring-8, with the approval of the Japan Synchrotron Radiation Research Institute (JASRI; Project No. 2024B1520).

Notes and references

1 M. Randić, *Chem. Rev.*, 2003, **103**, 3449–3606.
2 Z. Chen, C. S. Wannere, C. Corminboeuf, R. Puchta and P. von R. Schleyer, *Chem. Rev.*, 2005, **105**, 3842–3888.
3 A. T. Balaban, P. v. R. Schleyer and H. S. Rzepa, *Chem. Rev.*, 2005, **105**, 3436–3447.
4 M. Bendikov, F. Wudl and D. F. Perepichka, *Chem. Rev.*, 2004, **104**, 4891–4946.
5 J. E. Anthony, *Angew. Chem., Int. Ed.*, 2008, **47**, 452–483.
6 J. Mei, Y. Diao, A. L. Appleton, L. Fang and Z. Bao, *J. Am. Chem. Soc.*, 2013, **135**, 6724–6746.
7 Q. Ye and C. Chi, *Chem. Mater.*, 2014, **26**, 4046–4056.
8 G. Schweicher, G. Garbay, R. Jouclas, F. Vibert, F. Devaux and Y. H. Geerts, *Adv. Mater.*, 2020, **32**, 1905909.
9 C. Tönshoff and H. F. Bettinger, *Chem.–Eur. J.*, 2021, **27**, 3193–3212.
10 N. Zeitter, N. Hippchen, A. Weidlich, P. Jäger, P. Ludwig, F. Rominger, A. Dreuw, J. Freudenberg and U. H. F. Bunz, *Chem.–Eur. J.*, 2023, **29**, e202302323.
11 N. H. Zeitter Nikolai, P. Baur, T. V. Unterreiner, F. Rominger, J. Freudenberg and U. H. F. Bunz, *Org. Mater.*, 2024, **06**, 12–17.
12 C. Zong, S. Yang, Y. Sun, L. Zhang, J. Hu, W. Hu, R. Li and Z. Sun, *Chem. Sci.*, 2022, **13**, 11442–11447.
13 X. Liu, B. Chen, M. Wang, X. Gu and L. Zhang, *Angew. Chem., Int. Ed.*, 2025, **64**, e202416160.
14 R. Scholl, C. Seer and R. Weitzenböck, *Berichte Dtsch. Chem. Ges.*, 1910, **43**, 2202–2209.
15 E. Clar and Fr. John, *Berichte Dtsch. Chem. Ges. B Ser.*, 1930, **63**, 2967–2977.
16 E. Clar and R. Schoental, *Polycyclic Hydrocarbons*, London, Academic Press INC., 1964, vol. 1.
17 M. Solà, *Front. Chem.*, 2013, **1**, 22, DOI: 10.3389/fchem.2013.00022.
18 G. Portella, J. Poater and M. Solà, *J. Phys. Org. Chem.*, 2005, **18**, 785–791.
19 T. Jousselin-Oba, M. Mamada, K. Wright, J. Marrot, C. Adachi, A. Yassar and M. Frigoli, *Angew. Chem., Int. Ed.*, 2022, **61**, e202112794.
20 Y. Duan, G. Zhang, X. Liu, F. Shi, T. Wang, H. Yan, H. Xu and L. Zhang, *J. Org. Chem.*, 2022, **87**, 8841–8848.
21 X. Shi, T. Y. Gopalakrishna, Q. Wang and C. Chi, *Chem.–Eur. J.*, 2017, **23**, 8525–8531.
22 P. W. Fowler and W. Myrvold, *J. Phys. Chem. A*, 2011, **115**, 13191–13200.
23 S. Fias, P. W. Fowler, J. L. Delgado, U. Hahn and P. Bultinck, *Chem.–Eur. J.*, 2008, **14**, 3093–3099.
24 O. L. Griffith, A. G. Jones, J. E. Anthony and D. L. Lichtenberger, *J. Phys. Chem. C*, 2010, **114**, 13838–13845.
25 M. R. Ajayakumar, J. Ma and X. Feng, *Eur. J. Org Chem.*, 2022, **2022**, e202101428.
26 D. W. Szczepanik, M. Solà, T. M. Krygowski, H. Szatylowicz, M. Andrzejak, B. Pawełek, J. Dominikowska, M. Kukułka and K. Dyduch, *Phys. Chem. Chem. Phys.*, 2018, **20**, 13430–13436.
27 P. von R. Schleyer, M. Manoharan, H. Jiao and F. Stahl, *Org. Lett.*, 2001, **3**, 3643–3646.
28 J. E. Anthony, J. S. Brooks, D. L. Eaton and S. R. Parkin, *J. Am. Chem. Soc.*, 2001, **123**, 9482–9483.
29 Y. Gu, Y. G. Tullimilli, J. Feng, H. Phan, W. Zeng and J. Wu, *Chem. Commun.*, 2019, **55**, 5567–5570.
30 S. Zhang, F. Talnack, T. Jousselin-Oba, V. Bhat, Y. Wu, Y. Lei, Y. Tomo, H. Gong, L. Michalek, D. Zhong, C. Wu, A. Yassar, S. Mannsfeld, C. Risko, M. Frigoli and Z. Bao, *J. Mater. Chem. C*, 2023, **11**, 8992–9001.
31 L. Zhang, B. Walker, F. Liu, N. S. Colella, S. C. B. Mannsfeld, J. J. Watkins, T.-Q. Nguyen and A. L. Briseno, *J. Mater. Chem.*, 2012, **22**, 4266–4268.
32 L. Zhang, A. Fonari, Y. Zhang, G. Zhao, V. Coropceanu, W. Hu, S. Parkin, J.-L. Brédas and A. L. Briseno, *Chem.–Eur. J.*, 2013, **19**, 17907–17916.

33 F. Lirette, A. Darvish, Z. Zhou, Z. Wei, L. Renn, M. A. Petrukhina, R. T. Weitz and J.-F. Morin, *Chem. Sci.*, 2023, **14**, 10184–10193.
34 R. Gershoni-Poranne and A. Stanger, *Chem. Soc. Rev.*, 2015, **44**, 6597–6615.
35 T. M. Krygowski, *J. Chem. Inf. Comput. Sci.*, 1993, **33**, 70–78.
36 P. Ribar, L. Valenta, T. Šolomek and M. Juríček, *Angew. Chem., Int. Ed.*, 2021, **60**, 13521–13528.
37 R. Scholl and C. Seer, *Adv. Cycloaddit.*, 1912, **394**, 111–177.
38 J. Lee and J. Park, *Org. Lett.*, 2015, **17**, 3960–3963.
39 T. Jousselin-Oba, K. Sbargoud, G. Vaccaro, F. Meinardi, A. Yassar and M. Frigoli, *Chem.–Eur. J.*, 2017, **23**, 16184–16188.
40 K. Sbargoud, M. Mamada, T. Jousselin-Oba, Y. Takeda, S. Tokito, A. Yassar, J. Marrot and M. Frigoli, *Chem.–Eur. J.*, 2017, **23**, 5076–5080.
41 T. Jousselin-Oba, M. Mamada, A. Okazawa, J. Marrot, T. Ishida, C. Adachi, A. Yassar and M. Frigoli, *Chem. Sci.*, 2020, **11**, 12194–12205.
42 T. Jousselin-Oba, M. Mamada, J. Marrot, A. Maignan, C. Adachi, A. Yassar and M. Frigoli, *J. Am. Chem. Soc.*, 2019, **141**, 9373–9381.
43 J. H. Smith, D. Čavlović, L. T. Lackovic, M. Medina Lopez, E. Meirzadeh, M. L. Steigerwald, X. Roy, C. P. Nuckolls and S. R. Docherty, *J. Am. Chem. Soc.*, 2025, **147**, 111–117.
44 K. Fries, R. Walter and K. Schilling, *Adv. Cycloaddit.*, 1935, **516**, 248–285.
45 A. Ciesielski, T. M. Krygowski and M. K. Cyrański, *Symmetry*, 2010, **2**, 1390–1400.
46 A. Graovac, I. Gutman, M. Randic and N. Trinajstic, *J. Am. Chem. Soc.*, 1973, **95**, 6267–6273.
47 J. Oddershede and S. Larsen, *J. Phys. Chem. A*, 2004, **108**, 1057–1063.
48 M. Su, Y.-N. Jing, H. Bao and W.-M. Wan, *Mater Chem Front*, 2020, **4**, 2435–2442.
49 T. Friščić, R. W. Lancaster, L. Fábián and P. G. Karamertzanis, *Proc. Natl. Acad. Sci. U. S. A.*, 2010, **107**, 13216–13221.
50 J. Harada, N. Yoneyama, S. Sato, Y. Takahashi and T. Inabe, *Cryst. Growth Des.*, 2019, **19**, 291–299.
51 G. Portella, J. Poater, J. M. Bofill, P. Alemany and M. Solà, *J. Org. Chem.*, 2005, **70**, 2509–2521.
52 I. A. Titaley, D. M. Walden, S. E. Dorn, O. M. Ogba, S. L. Massey Simonich and P. H.-Y. Cheong, *Environ. Sci. Technol.*, 2019, **53**, 1595–1607.
53 B. K. Shah, D. C. Neckers, J. Shi, E. W. Forsythe and D. Morton, *J. Phys. Chem. A*, 2005, **109**, 7677–7681.
54 G. Markert, E. Paenurk and R. Gershoni-Poranne, *Chem.–Eur. J.*, 2021, **27**, 6923–6935.
55 R. K. Dubey, M. Marongiu, S. Fu, G. Wen, M. Bonn, H. I. Wang, M. Melle-Franco and A. Mateo-Alonso, *Chem*, 2023, **9**, 2983–2996.
56 W. P. Partridge, N. M. Laurendeau, C. C. Johnson and R. N. Steppel, *Opt. Lett.*, 1994, **19**, 1630–1632.
57 O. Nagler, A.-M. Krause, K. Shoyama, M. Stolte, R. K. Dubey, L. Liu, Z. Xie and F. Würthner, *Org. Lett.*, 2022, **24**, 6839–6844.
58 Y. Jue Bae, M. D. Krzyaniak, M. B. Majewski, M. Desroches, J.-F. Morin, Y.-L. Wu and M. R. Wasielewski, *ChemPlusChem*, 2019, **84**, 1432–1438.
59 D. J. Stewart, J. Shi, T. R. Naranjo, T. A. Grusenmeyer, J. M. Artz, C. L. McCleese, R. M. O'Donnell, T. M. Cooper, W. M. Shensky and J. E. Haley, *Phys. Chem. Chem. Phys.*, 2018, **20**, 28412–28418.
60 Y. Bo, N. Zink-Lorre, R. Weiß, Á. Sastre-Santos, T. Clark, F. Fernández-Lázaro and D. M. Guldi, *Artif. Photosynth*, 2025, **1**, 226–236.
61 M. Dvořák, S. K. K. Prasad, C. B. Dover, C. R. Forest, A. Kaleem, R. W. MacQueen, A. J. I. Petty, R. Forecast, J. E. Beves, J. E. Anthony, M. J. Y. Tayebjee, A. Widmer-Cooper, P. Thordarson and T. W. Schmidt, *J. Am. Chem. Soc.*, 2021, **143**, 13749–13758.
62 K. Yamaguchi, *Chem. Phys. Lett.*, 1975, **33**, 330–335.
63 M. Nakano, R. Kishi, T. Nitta, T. Kubo, K. Nakasuji, K. Kamada, K. Ohta, B. Champagne, E. Botek and K. Yamaguchi, *J. Phys. Chem. A*, 2005, **109**, 885–891.
64 J. Ly, K. Martin, S. Thomas, M. Yamashita, B. Yu, C. A. Pointer, H. Yamada, K. R. Carter, S. Parkin, L. Zhang, J.-L. Bredas, E. R. Young and A. L. Briseno, *J. Phys. Chem. A*, 2019, **123**, 7558–7566.
65 (*a*) CCDC 2503087: Experimental Crystal Structure Determination, 2026, DOI: 10.5517/ccdc.csd.cc2q0nr5; (*b*) CCDC 2503088: Experimental Crystal Structure Determination, 2026, DOI: 10.5517/ccdc.csd.cc2q0ns6; (*c*) CCDC 2504051: Experimental Crystal Structure Determination, 2026, DOI: 10.5517/ccdc.csd.cc2q1nv9.